

MLLM4PUE: Toward Universal Embeddings in Computational Pathology through Multimodal LLMs

Qifeng Zhou Thao M. Dang Wenliang Zhong Yuzhi Guo
 Hehuan Ma Saiyang Na Junzhou Huang*
 The University of Texas at Arlington

Abstract

Pathology plays a critical role in diagnosing a wide range of diseases, yet existing approaches often rely heavily on task-specific models trained on extensive, well-labeled datasets. These methods face sustainability challenges due to the diversity of pathologies and the labor-intensive nature of data collection. To address these limitations, we highlight the need for universal multimodal embeddings that can support multiple downstream tasks. Previous approaches often involve fine-tuning CLIP-based models, which handle images and text separately, limiting their ability to capture complex multimodal relationships. Additionally, these models are evaluated across diverse datasets without a unified benchmark for assessing multimodal embeddings in pathology. To address these challenges, we propose MLLM4PUE, a novel framework that leverages Multimodal Large Language Models (MLLMs) to generate Pathology Universal Embeddings. The MLLM4PUE framework not only facilitates robust integration of images and text but also enhances understanding and fusion capabilities across various tasks. We further introduce the Pathology Multimodal Embedding Benchmark (PMEB), a comprehensive benchmark designed to assess the quality of pathology multimodal embeddings. PMEB comprises 15 original tasks drawn from 14 datasets, organized into three meta-tasks: retrieval, classification, and composed retrieval. Experimental results demonstrate the superiority of MLLM4PUE, illustrating MLLM-based models can effectively support a wide range of downstream tasks and unify the research direction for foundation models in pathology.

1. Introduction

Pathology remains the gold standard for diagnosing a wide range of diseases [8, 32, 42]. With rapid advancements in artificial intelligence (AI), computational pathology has emerged as a promising field, using AI to ad-

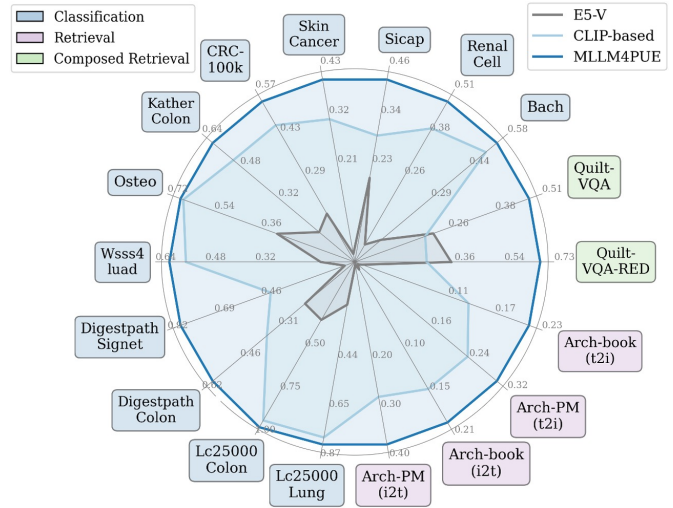


Figure 1. Performance comparison across benchmark datasets, showing that our proposed MLLM4PUE achieves state-of-the-art (SOTA) results across all tasks. Weight F1 (wF1) is reported for classification task. For the retrieval and composed retrieval task, we report recall@5 scores. This highlights the advanced multimodal fusion capabilities of MLLM4PUE.

dress challenges across various tasks such as cancer diagnosis [29, 39], metastasis detection [22, 44], mutation prediction [9, 33, 37], and survival analysis [40, 41, 45]. These achievements, however, rely on task-specific models trained on large, well-labeled datasets. Given the hundreds of tumor types cataloged in the WHO classification¹ and the labor-intensive nature of data collection and annotation [12], developing separate, high-performing models for each pathology task is impractical, especially for rare diseases with limited data [24, 30]. Furthermore, while many efforts focus on image data, pathology often involves natural language, including diagnostic reports and research publications [6, 7, 14, 31]. Thus, there is a growing need to shift toward task-agnostic models that generate universal multi-

*Corresponding author: jzhuang@uta.edu

¹tumourclassification.iarc.who.int/

modal embeddings capable of supporting a broad range of pathology tasks.

In natural image processing, recent studies such as CLIP [34] have demonstrated remarkable success by aligning visual and language embeddings through contrastive learning, achieving strong performance across diverse downstream tasks. Building on these advances, several studies [16, 17, 30, 31, 38] have adapted CLIP-based models for pathology, training on extensive image-text pairs from public sources to produce multimodal embeddings that enable zero-shot learning across various pathology tasks. However, these methods encounter two significant challenges. First, CLIP [34] processes images and text independently, limiting its ability to capture complex interactions between modalities [19]. Second, evaluations of these models have mostly centered on isolated tasks, such as classification or retrieval [17, 30, 38], which separate image and text components and do not fully assess multimodal integration capabilities. Moreover, inconsistencies in datasets and sample selection criteria across studies lead to non-reproducible and incomparable results, emphasizing the need for a more integrated approach and a standardized benchmarking framework to advance multimodal embeddings in pathology.

To tackle the first challenge, we propose MLLM4PUE, a framework that uses a Multimodal Large Language Model (MLLM) backbone to generate universal multimodal embeddings for pathology. To the best of our knowledge, this is the first use of an MLLM backbone in this field, representing a significant advancement over previous CLIP-based methods. Unlike CLIP [34], which processes images and text separately, MLLM4PUE employs a transformer-based architecture to fully integrate these modalities, allowing it to learn from complex image-text relationships. This fusion enhances the model’s adaptability and effectiveness across a range of pathology tasks, making it particularly suited for generalizing to diverse pathology scenarios [27, 28].

To address the second challenge, we introduce the Pathology Multimodal Embedding Benchmark (PMEB) to establish a standardized evaluation platform for multimodal embeddings in pathology. This benchmark encompasses three meta-task categories: retrieval, composed retrieval, and classification. To ensure the tasks effectively assess multimodal embeddings, we have reformulated them to better suit this purpose. Each task provides the model with prompts to process a query and identify the correct target from a set of candidates. These queries and targets can consist of images, text, or a combination of both, enabling a flexible and comprehensive evaluation of multimodal capabilities. PMEB offers a standardized and reproducible approach for assessing multimodal embeddings in pathology. Overall, our contributions are summarized as follows:

- We introduce MLLM4PUE, the first framework utilizing MLLMs to generate universal multimodal embeddings in pathology. This framework integrates multimodal information within a unified model, converting any combination of images and text into robust embeddings.
- We provide PMEB, a comprehensive benchmark for evaluating multimodal embeddings in pathology, encompassing a broad range of tasks to support robust and generalizable assessment of these embeddings.
- MLLM4PUE effectively represents multimodal information, consistently surpassing the performance of all baseline models across all evaluated tasks, as demonstrated by the quantitative results in Fig. 1.
- Our approach offers new insights into computational pathology by adopting MLLMs for universal embeddings. Future research can build on this work to unify and streamline the development of models for diverse pathology tasks.

2. Related work

2.1. Multimodal embedding learning

Creating effective multimodal embeddings remains a challenging area of research. The CLIP model [34] addresses this by employing separate encoders for images and text, aligning them in a common space through contrastive learning. This approach has influenced many subsequent models, such as BLIP [26] and CoCa [43]. While these models excel in a variety of tasks, the use of distinct encoders restricts their capacity to fully integrate visual and textual data, which is a key requirement for tasks that involve combined visual-language inputs, such as search queries involving both images and text.

With the rise of large language models (LLMs), Multimodal Large Language Models (MLLMs) have extended LLMs to process multiple data modalities, achieving notable progress in understanding and reasoning across diverse input types [25, 27, 28]. Although MLLMs exhibit strong capabilities in interpreting multimodal content and following complex instructions, there is still limited research on their application in creating effective multimodal embeddings. The recent E5-V [19] model fine-tunes MLLMs with text-based data to improve embedding quality. Building on this, we have adapted the approach for pathology by using domain-specific image-text data, resulting in substantial performance improvements.

2.2. Multimodal embeddings for computational pathology

In computational pathology, recent studies have adopted the CLIP [34] architecture and training methodology, leveraging paired image-text data within a contrastive learning framework to align similar image-text embeddings

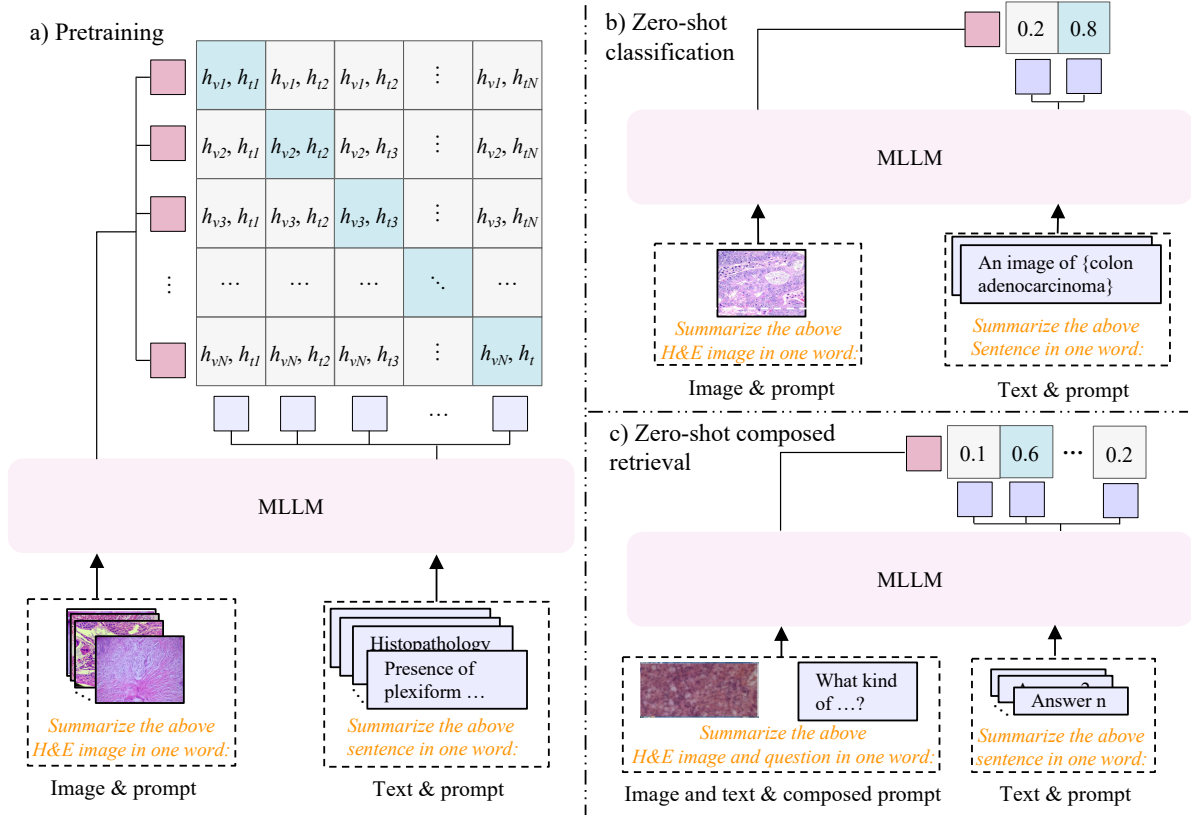


Figure 2. Overview of the MLLM4PUE framework. (a) Illustration of pathology image-text contrastive learning with our proposed method. With different prompts, MLLM can generate embeddings for multimodal inputs. Image and text embeddings are aligned using a contrastive loss. (b) Zero transfer for classification. (c) Zero transfer for composed retrieval.

while separating dissimilar ones [16–18, 30, 38]. For instance, PLIP [16] fine-tunes CLIP on large collections of image-text pairs sourced from platforms like Twitter and other public datasets. Similarly, PathCLIP [38] and Quilt-Net [17] scale up pathology-specific data for fine-tuning, while CONCH [31] employs over 1.17 million image-caption pairs, making it the largest dataset used for training to date.

Despite these advancements, these methods fine-tune either CLIP [34] or CoCa [43] using pathology image-caption pairs and rely on separate encoders for processing images and text. In contrast, we propose an MLLM-based approach to capture universal multimodal embeddings for pathology by integrating image and text data within a unified model. This integrated framework enhances performance across a wide range of computational pathology tasks, offering a more holistic and effective solution.

3. Methodology

In this section, we first introduce the Pathology Multimodal Embedding Benchmark (PMEB), a comprehensive benchmark for evaluating multimodal embeddings in di-

verse pathology tasks. Then, we present the MLLM4PUE framework, which integrates multimodal embeddings, contrastive learning, and zero-shot transfer methods to align and adapt pathology image-text data effectively, as illustrated in Fig. 2.

3.1. Pathology multimodal embedding benchmark

We propose PMEB (Pathology Multimodal Embedding Benchmark), a comprehensive benchmark designed to evaluate multimodal embeddings in pathology across a diverse range of tasks. These tasks include cancer tissue classification [2, 4, 23], Gleason pattern grading [36], and cell identification [10], among other tasks. PMEB comprises 15 original tasks from 14 datasets, organized into three meta-tasks: retrieval, classification, and composed retrieval. All tasks are reformulated to assess multimodal embeddings, where the model receives an instructional prompt and a query, which may consist of text, images, or both, and selects the correct target from a set of options.

In the retrieval task, the query can be either an image or text, with the target being the corresponding paired text or image. For the classification task, queries are images with

Meta-Task	Data source	Query	Target	Original Tasks	Original samples	Selected samples
Retrieval	Arch-book [13]	I	T	Image-text retrieval	1,306	1,306
	Arch-book [13]	T	I	Text-image retrieval	1,306	1,306
	Arch-pubmed [13]	I	T	Image-text retrieval	1,923	1,923
	Arch-pubmed [13]	T	I	Text-image retrieval	1,923	1,923
Composed retrieval	Quilt-VQA [35]	I+T	T	Histopathology VQA	985	724
	Quilt-VQA-RED [35]	I+T	T	Histopathology VQA	335	252
Classification	Bach [2]	I	T	Breast tissue	399	399
	CRC-100k [20]	I	T	Colorectal cancer	100,000	1,500
	Digestpath [10]	I	T	Signet ring cell	455	455
	Digestpath [10]	I	T	Colonoscopy tissue	660	660
	Kathercolon [21]	I	T	Colorectal cancer tissue	7,180	1,500
	LC25000 [4]	I	T	Colon adenocarcinoma	10,000	1,500
	LC25000 [4]	I	T	Lung adenocarcinoma	15,000	1,500
	Osteo [3]	I	T	Osteosarcoma	1,144	1,144
	Renalcell [5]	I	T	Renal tissue	36,687	1,500
	Sicap [36]	I	T	Gleason pattern	12,081	1,500
	Skincancer [23]	I	T	Skin cancer tissue	129,369	1,500
	Wsss4luad [15]	I	T	LUAD tissue	4,693	1,500

Table 1. The statistics of our PMEB benchmark: 15 original tasks from 14 datasets. I and T denote image and text, respectively.

targets as text labels representing various classes. The composed retrieval task involves queries that combine an image with text formatted as a question, with the target being the expected answer. This composed retrieval task, specifically designed for multimodal embedding evaluation, incorporates integrated visual and language inputs and has not been applied in previous methods. Detailed dataset statistics are provided in Table 1.

Due to the large size of certain classification datasets, we have standardized their sizes. For datasets containing more than 1,500 samples, we employ the CONCH model [31] to calculate similarity scores between each image and its corresponding class label text. We then select the top 500 images with the highest scores, the bottom 500 with the lowest scores, and a random sample of 500 from the remaining data, ensuring the original category distribution is preserved. For the composed retrieval task, we select only open-ended questions from the data source, where answers are more complex than a simple “yes” or “no”. Additionally, since there is an overlap between questions and answers in the VQA data source, we utilize ChatGPT [1] for data cleaning to ensure clarity and accuracy in task evaluation. Further details and examples from each dataset within PMEB are provided in Supplementary Materials.

3.2. Multimodal Embeddings with MLLM

We first introduce how our proposed MLLM4PUE leverages MLLMs for universal multimodal embedding learning. Unlike CLIP, which directly generates embeddings for multimodal inputs, MLLMs are inherently generative models and require a different approach to produce embeddings. Inspired by E5-V [19], our solution uses a prompt-based

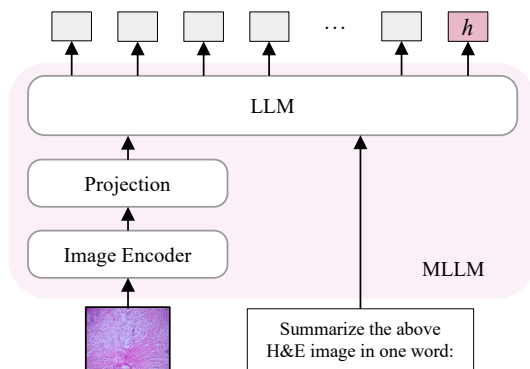


Figure 3. Illustration of the MLLM4PUE framework for generating multimodal embeddings using an MLLM. The image is processed through an Image Encoder and projection layer, with a prompt guiding the MLLM to distill the image content into a single-word embedding. The final embedding h is extracted from the last token as the unified multimodal representation.

strategy specifically designed to guide MLLMs in embedding multimodal data.

Given an MLLM f_φ parameterized by φ , and a query q , we employ the following prompt, $\langle q \rangle \backslash n$ Summarize above $\langle \rangle$ in one word:, to generate the input q_{input} . In this setup, $\langle q \rangle$ serves as a placeholder for the query, while $\langle \rangle$ indicates the type of the query’s content. For instance, if query q is an image, the prompt would be $\langle image \rangle \backslash n$ Summarize above H&E image in one word:; if query q is a sentence, then the prompt would be $\langle text \rangle \backslash n$ Summarize above sentence in one word:.

The prompt design incorporates two components: first,

the word `Summarize` directs the MLLM to distill the information of the multimodal input. The second part, `in one word:`, instructs the MLLM to compress this distilled information into a single token, thereby facilitating a unified multimodal embedding. Once the extended input q_{input} is constructed, it is processed by the MLLM f_φ to generate embeddings: $h = f_\varphi(q_{input})$, where h is the embedding of last token obtained from the MLLM output, as illustrated in Fig. 3. This approach tailors the generation capabilities of MLLMs to effectively produce and utilize multimodal embeddings, expanding their application potential beyond traditional generative outputs.

3.3. Pathology Contrastive Learning

Next, we describe the approach for projecting pathological data into a latent embedding space using conservative learning. As illustrated in Fig. 2, given a batch of N paired image and text samples $\{(v_n, t_n)\}_{n=1, \dots, N}$ and MLLM f_φ , for each sample (v_i, t_i) , we feed them into f_φ to get the image and text embeddings (h_{v_i}, h_{t_i}) as described in Sec. 3.2.

The objective is to build a latent space for pathology image-text embeddings that maximizes the similarity between embeddings of the paired samples in the batch, while minimizing the similarity between embeddings of the $N - 1$ incorrect pairs. We optimize an infoNCE contrastive Loss \mathcal{L} to train our model.

$$\mathcal{L} = -\left(\log \frac{e^{\cos(h_{v_i}, h_{t_i})/\tau}}{\sum_{j=1}^n e^{\cos(h_{v_i}, h_{t_j})/\tau}} + \log \frac{e^{\cos(h_{t_i}, h_{v_i})/\tau}}{\sum_{j=1}^n e^{\cos(h_{t_i}, h_{v_j})/\tau}}\right), \quad (1)$$

where τ is a temperature parameter and $\cos(h_{v_i}, h_{t_i})$ and $\cos(h_{t_i}, h_{v_i})$ represent the cosine similarity in both directions in contrastive learning.

3.4. Zero-shot Transfer Evaluation

Our model, trained primarily on retrieval tasks focused on image-text pairs, requires adaptation to handle zero-shot classification and composed retrieval tasks. The details of how we modify the model for these different zero-shot downstream tasks are introduced as follows.

For zero-shot classification, we adopt a prompt-based method inspired by the CLIP model [34]. In this approach, each class name is expanded into a sentence using a specific template. For instance, the class name ‘‘Colon adenocarcinoma’’ is converted into the sentence ‘‘An H&E image of Colon adenocarcinoma’’ using the template ‘‘An H&E image of { }.’’ We apply this method to create sentences for all class names. Our model then computes embeddings for these sentences and the test images, extracting the last token of the MLLM output as described in Section 3.2. The similarity between these embeddings is calculated as outlined in Section 3.3, and test image labels are assigned based on the highest similarity scores. To account for variability in templates, we randomly select one from the 21 templates

in CONCH [31] and repeat this process 100 times for each dataset. The templates are exhibited in Supplementary Materials.

For the composed retrieval task, where the query consists of both an image and a question, we need to convert this multimodal information into a unified embedding. Thus, we use the prompt `<image>\n <question>\n Summarize above H&E image and question in one word:` to integrate the image and the question. Our model then generates embeddings for this combined input, as explained in Section 3.2, which are used to retrieve the embeddings of the corresponding answers.

4. Experiments

4.1. Training Datasets

We leverage three public datasets, Openpath [16], PathCap [38] and Quilt1M [17], to construct a robust training foundation for pathology image-text pairs.

The Openpath dataset [16] is assembled by gathering data from Twitter and LAION using popular pathology hashtags. Since PLIP[16] provided only Twitter IDs, we retrieve the corresponding data from Twitter and LAION using these IDs, resulting in a dataset of 138,874 image-text pairs after denoising. The PatchCap dataset [38] comprises 207K high-quality samples from authoritative sources, and we use all provided image-text samples. Similarly, the Quilt1M dataset [17] aggregates pathology image-text pairs from several public sources. As many images in Quilt1M are associated with multiple captions, we concatenate the captions for each image to create comprehensive entries. Through these careful preparations, we compile an extensive training dataset consisting of 593,838 image-text pairs.

4.2. Baselines

We evaluate the performance of our proposed MLLM4PUE, against several recent SOTA approaches across various downstream tasks. Specifically, we compare with three currently developed CLIP-based methods: PLIP [16], PathCLIP [38], and QuiltNet [17]. We also compare our method with E5-V [19], a contemporary model that leverages vision-language models for multimodal embedding tasks. It proposes a single-modality training approach, where the model is trained exclusively on text pairs.

4.3. Implementation Details and Metrics

We use LLaVA-NeXT [25] as our backbone MLLM. To save the GPU memory, we use QLoRA [11] and gradient checkpointing with DeepSpeed ZeRO-2, and all the images are resized to 336×336 pixels. The temperature is set to 0.02. All experiments are run on six H100 GPUs.

To evaluate the performance of retrieval and composed retrieval tasks, we use the Recall@K metric, which quan-

Task	Model	Arch-PubMed [13]			Arch-book [13]		
		Recall@5	Recall@10	Recall@50	Recall@5	Recall@10	Recall@50
i2t	E5-V [19]	0.006	0.011	0.052	0.009	0.018	0.067
	PLIP [16]	0.037	0.067	0.185	0.096	0.152	0.393
	MLLM4PUE-O	0.105	0.160	0.366	0.185	0.264	0.575
	PathCLIP [17]	0.275	0.388	0.680	0.152	0.234	0.482
	MLLM4PUE-P	0.372	0.495	0.782	0.192	0.283	0.603
	QuiltNet [17]	0.069	0.111	0.273	0.116	0.168	0.384
	MLLM4PUE-Q	0.122	0.177	0.407	0.182	0.248	0.502
t2i	E5-V [19]	0.006	0.011	0.052	0.009	0.018	0.067
	PLIP [16]	0.037	0.067	0.181	0.112	0.164	0.419
	MLLM4PUE-O	0.114	0.173	0.385	0.193	0.280	0.600
	PathCLIP [17]	0.236	0.348	0.630	0.137	0.196	0.445
	MLLM4PUE-P	0.297	0.399	0.688	0.185	0.277	0.555
	QuiltNet [17]	0.056	0.092	0.237	0.100	0.152	0.389
	MLLM4PUE-Q	0.135	0.193	0.433	0.210	0.302	0.584

Table 2. Performance comparison with baseline methods on two retrieval datasets, reporting recall metrics at different thresholds. Task i2t and t2i denote image-to-text and text-to-image retrieval, respectively. MLLM4PUE-O, MLLM4PUE-P, and MLLM4PUE-Q denote our model pre-trained on Openpath [16], PathCap [38], Quilt1M [17], respectively. Bold values indicate the best performance.

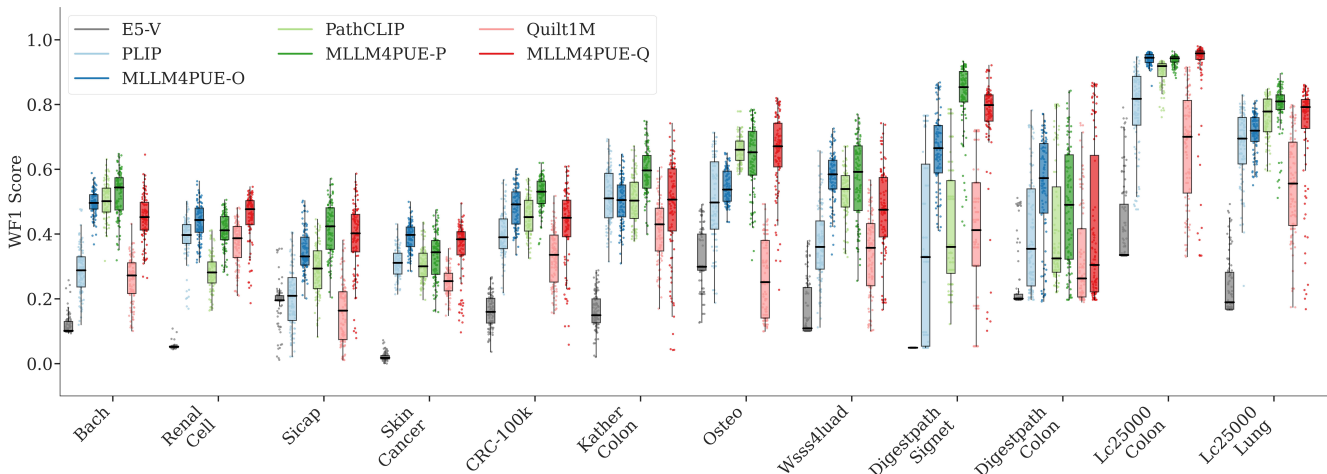


Figure 4. Comparison of zero-shot patch classification performance across different models, measured by weighted F1 metric. Each box represents 100 data points, with each point indicating the performance on one template. The upper, middle, and lower lines of each box denote the first, median, and third quartiles, respectively. MLLM4PUE-O, MLLM4PUE-P, and MLLM4PUE-Q denote our model pre-trained on Openpath [16], PathCap [38], Quilt1M [17], respectively.

ifies the proportion of relevant items contained within the top K retrieved results. For classification tasks, due to the imbalanced distribution of classes, we use the weighted F1 (wF1) score to assess performance. The weighted F1 is calculated by averaging the F1 scores for each class, with each class’s score weighted by its frequency of occurrence.

5. Results

5.1. Zero-shot Cross-modal Retrieval

We first evaluate our methods on the retrieval task, where the query is an image or text, with the target being the corresponding paired text or image. Recall@ k metric is

employed to assess the model’s ability to retrieve relevant pathology image-text pairs among top k results. Our MLLM4PUE models are pre-trained on Openpath [16], PatchCap [38], and Quilt1M [17]. As shown in Table 2, our models consistently outperform the baseline models, especially at higher recall values. Notably, in the image-to-text (i2t) task on Arch-book dataset [13], our MLLM4PUE trained on Openpath dataset [16] achieves a Recall@5 of 0.185, indicating an approximate 9% improvement over PLIP [16]. Moreover, our PathCap-pretrained model surpasses the performance of PathCLIP [38] on both benchmark datasets. A similar enhancement is observed in the text-to-image (t2i) retrieval task. For instance, on the Arch-

Model	Quilt-VQA [35]			Quilt-VQA-RED [35]		
	Recall@5	Recall@10	Recall@50	Recall@5	Recall@10	Recall@50
E5-V [19]	0.214	0.323	0.495	0.351	0.441	0.668
PLIP [16]	0.191	0.224	0.349	0.250	0.286	0.500
MLLM4PUE-O	0.239	0.334	0.583	0.373	0.460	0.790
PathCLIP [17]	0.192	0.242	0.413	0.262	0.337	0.603
MLLM4PUE-P	0.218	0.329	0.541	0.363	0.468	0.790
QuiltNet [17]	0.180	0.209	0.336	0.222	0.274	0.460
MLLM4PUE-Q	0.475	0.598	0.823	0.675	0.754	0.948

Table 3. Zero-shot composed retrieval performance on the Quilt-VQA and Quilt-VQA-RED datasets, with Recall metrics reported at various thresholds. MLLM4PUE-O, MLLM4PUE-P, and MLLM4PUE-Q denote our model pre-trained on Openpath [16], PathCap [38], Quilt1M [17], respectively. Bold values indicate the best performance.

Prompt-tuning	Prompt	Arch-PubMed [13]				Arch-book [13]			
		i2t		t2i		i2t		t2i	
		R@5	R@10	R@5	R@10	R@5	R@10	R@5	R@10
no	no prompt	0.086	0.135	0.087	0.137	0.147	0.213	0.149	0.226
	no “in one word”	0.092	0.137	0.095	0.142	0.152	0.236	0.158	0.233
yes	no prompt	0.091	0.139	0.091	0.141	0.152	0.233	0.161	0.246
	no “in one word”	0.094	0.143	0.102	0.149	0.157	0.243	0.165	0.258
	MLLM4PUE	0.098	0.155	0.109	0.162	0.169	0.253	0.177	0.274

Table 4. Impact of prompt-tuning on two retrieval datasets. All models are trained on the Openpath dataset [16] for 1000 steps. Task i2t and t2i denote image-to-text and text-to-image retrieval. R@5 and R@10 represent Recall@5 and Recall@10, respectively. Bold values indicate the best performance.

Model		Quilt-VQA [13]			Quilt-VQA-RED [13]		
		Recall@5	Recall@10	Recall@50	Recall@5	Recall@10	Recall@50
QuiltNet [17]	only question	0.170	0.189	0.275	0.187	0.234	0.440
	add embedding	0.180	0.209	0.336	0.222	0.274	0.460
MLLM4PUE	only question	0.291	0.362	0.539	0.429	0.488	0.694
	add embedding	0.394	0.500	0.746	0.520	0.619	0.909
	prompt	0.475	0.598	0.823	0.675	0.754	0.948

Table 5. Ablation study of image and question embedding fusion methods on composed retrieval task. All models are trained on the Quilt1M [17] dataset. Recall metrics are reported. Bold values indicate the best performance.

PubMed dataset [13], our model achieves a Recall@10 of 0.193, marking a 10% increase in performance. These results collectively demonstrate that our framework excels at capturing multimodal embeddings more effectively than CLIP-based models with the same training data. Furthermore, it is important to note that the E5-V model [19], although sharing the same underlying architecture as ours, yields significantly lower recall scores across all tasks and datasets due to the lack of fine-tuning with pathology-specific data.

5.2. Zero-shot Patch Classification

We then evaluate the performance of zero-shot classification on patch-level pathology images. Specifically, each query is an image, and the target is an extended sentence of the class name, constructed using a template outlined in sec 3.4. Following CONCH [31], we conduct 100 experimental trials

for each dataset, randomly selecting one template from a set of 21 templates for each trial. The detailed descriptions are available in the Supplementary Material. We present the distribution of weighted F1 scores (wF1) from these 100 experiments in Fig. 4, where the top, middle, and bottom lines of each box depict the first quartile, median, and third quartile of the wF1 score distribution, respectively. Each point in the figure indicates a single template’s performance.

Fig. 4 illustrates that our MLLM4PUE consistently surpasses baseline models trained on identical datasets. For instance, in the “DigestpathSignet” task with the Openpath dataset [16], which focuses on identifying signet ring cells, MLLM4PUE-O achieves a median wF1 score of 0.665, marking an improvement of over 30% compared to PLIP’s median of 0.329. When the training data changes to PathCLIP [38], MLLM4PUE-P also shows considerable advancements, achieving a median score of 0.854 compared

to PathCLIP’s 0.361. This implies a performance increase of roughly 50%. Similarly, using the QuiltNet dataset [17], MLLM4PUE-Q excels in the “Sicap” dataset, reaching a median wF1 of 0.402, far exceeding QuiltNet’s 0.164. In the “Osteo” dataset, MLLM4PUE-Q achieves a median wF1 score of 0.671, significantly outclassing QuiltNet with an improvement exceeding 40%. Moreover, when compared with E5V, MLLM4PUE demonstrates superior performance, delivering higher wF1 scores even with the same architectural foundation. These results confirm the superiority of MLLM4PUE in enhancing zero-shot classification performance through effective multimodal data integration, establishing it as a robust choice for various pathology image classification tasks.

5.3. Zero-shot Composed Retrieval

We further evaluate the performance of composed retrieval on two datasets, where the task involves using an image and a question as the query to retrieve the correct answer. The Recall@k metric is employed to assess how well the model can identify the correct answer within the top k candidates. As shown in Table 3, our proposed MLLM4PUE demonstrates significant improvements compared to baseline methods, even when trained with the same pre-training data. Specifically, on the Quilt-VQA dataset [35], MLLM4PUE achieves an increase in Recall@5 by approximately 4%, 3%, and 30% over PLIP [16], PathCLIP [38], and QuiltNet [17], respectively. Similarly, on the Quilt-RED-VQA dataset [35], MLLM4PUE pre-trained on Quilt1M [17], has achieved a Recall@5 of 0.675, which represents the best performance among all baseline methods. Interestingly, the E5-V model [19] exhibits superior performance compared to all CLIP-based models, despite lacking fine-tuning on pathology-specific data. This demonstrates the robust capacity of MLLM backbone in multimodal embedding fusion, highlighting its proficiency in handling diverse data inputs effectively.

5.4. Ablation studies

5.4.1. Impact of Prompts

To assess the impact of different prompt strategies, we conduct a comparative analysis between our MLLM4PUE and two alternative approaches: no prompt - where images or text are directly input into the model without prompts, and no “in one word” - employing a similar prompt to our method but omitting the phrase “in one word”. Table 4 presents the performance of these methods, both with and without fine-tuning. All models are trained on Openpath dataset [16] for 1000 steps. For models employing fine-tuning, each method is adjusted with its respective prompts. In contrast, the no fine-tuning scenario involves simply altering the prompt for the already finely-tuned MLLM4PUE model. Our method shows significant improvements on

zero-shot retrieval tasks compared to the no prompt and no “in one word”. For the Arch-PubMed dataset, MLLM4PUE attains Recall@5 scores of 0.098 and 0.109 for image-to-text and text-to-image tasks, respectively, marking the best performance in those categories. Similarly, in the Arch-book dataset, MLLM4PUE achieves the top Recall@5 and Recall@10 scores, indicating superior retrieval effectiveness. These results highlight the significant enhancements provided by our prompt, emphasizing its role in facilitating more accurate zero-shot retrieval in complex datasets by better aligning multimodal inputs.

5.4.2. Fusion Method in Composed Retrieval

This experiment is designed to highlight the effectiveness of our MLLM4PUE in modality fusion while exploring the limitations of CLIP in handling composed retrieval tasks. As shown in Table 5, the results reveal that QuiltNet [17], a CLIP-based model, shows little difference in performance between using only the question text and integrating image embeddings. This indicates that CLIP’s method lacks robust modality integration, as the inclusion of visual information fails to significantly enhance its effectiveness. Conversely, our model, MLLM4PUE, demonstrates substantial improvements by effectively fusing image and text information. MLLM4PUE outperforms QuiltNet in every setting. The true strength of our approach becomes evident when employing a prompt-based method, leading to significantly higher recall scores. Specifically, it achieves Recall@5 values of 0.475 on Quilt-VQA and 0.675 on Quilt-VQA-RED, representing approximately an 8% and 12% improvement over the simple addition method, respectively, and an 18% and 25% improvement over using the question text alone.

These findings clearly indicate that our model’s ability to integrate both visual and textual modalities results in significant enhancements in retrieval accuracy. This surpasses both mere modality addition and the question-only configuration, highlighting the effectiveness of our modality fusion technique for composed retrieval tasks. Our approach provides advantages that cannot be achieved through separate handling or limited integration of text and image data.

6. Conclusion

In conclusion, our work represents a significant advancement in different downstream tasks through MLLM4PUE, a novel framework leveraging MLLMs to achieve universal multimodal embeddings. By effectively integrating image and text data, our model addresses the limitations of previous CLIP-based methods. We also introduce PMEB, which provides a standardized and comprehensive benchmark for evaluating multimodal capabilities, promoting reproducibility and comparability in the field. This study also paves the way for future research to utilize MLLM-based models to support a wide range of downstream tasks and unify the research direction for foundation models in pathology.

References

- [1] Josh Achiam, Steven Adler, Sandhini Agarwal, Lama Ahmad, Ilge Akkaya, Florencia Leoni Aleman, Diogo Almeida, Janko Altenschmidt, Sam Altman, Shyamal Anadkat, et al. Gpt-4 technical report. *arXiv preprint arXiv:2303.08774*, 2023. 4
- [2] Guilherme Aresta, Teresa Araújo, Scotty Kwok, Sai Saketh Chennamsetty, Mohammed Safwan, Varghese Alex, Bahram Marami, Marcel Prastawa, Monica Chan, Michael Donovan, et al. Bach: Grand challenge on breast cancer histology images. *Medical image analysis*, 56:122–139, 2019. 3, 4
- [3] Harish Babu Arunachalam, Rashika Mishra, Ovidiu Daescu, Kevin Cederberg, Dinesh Rakheja, Anita Sengupta, David Leonard, Rami Hallac, and Patrick Leavey. Viable and necrotic tumor assessment from whole slide images of osteosarcoma using machine-learning and deep-learning models. *PLoS one*, 14(4):e0210706, 2019. 4
- [4] Andrew A Borkowski, Marilyn M Bui, L Brannon Thomas, Catherine P Wilson, Lauren A DeLand, and Stephen M Mastorides. Lung and colon cancer histopathological image dataset (lc25000). *arXiv preprint arXiv:1912.12142*, 2019. 3, 4
- [5] Otso Brummer, Petri Pölönen, Satu Mustjoki, and Oscar Brück. Integrative analysis of histological textures and lymphocyte infiltration in renal cell carcinoma using deep learning. *bioRxiv*, pages 2022–08, 2022. 4
- [6] Pingyi Chen, Honglin Li, Chenglu Zhu, Sunyi Zheng, Zhongyi Shui, and Lin Yang. WsiCaption: Multiple Instance Generation of Pathology Reports for Gigapixel Whole-Slide Images. In *proceedings of Medical Image Computing and Computer Assisted Intervention – MICCAI 2024*. Springer Nature Switzerland, 2024. 1
- [7] Pingyi Chen, Chenglu Zhu, Sunyi Zheng, Honglin Li, and Lin Yang. Wsi-vqa: Interpreting whole slide images by generative visual question answering. In *European Conference on Computer Vision*, pages 401–417. Springer, 2025. 1
- [8] Richard J Chen, Chengkuan Chen, Yicong Li, Tiffany Y Chen, Andrew D Trister, Rahul G Krishnan, and Faisal Mahmood. Scaling vision transformers to gigapixel images via hierarchical self-supervised learning. In *Proceedings of the IEEE/CVF Conference on Computer Vision and Pattern Recognition*, pages 16144–16155, 2022. 1
- [9] Nicolas Coudray, Paolo Santiago Ocampo, Theodore Sakellaropoulos, Navneet Narula, Matija Snuderl, David Fenyö, Andre L Moreira, Narges Razavian, and Aristotelis Tsirigos. Classification and mutation prediction from non-small cell lung cancer histopathology images using deep learning. *Nature medicine*, 24(10):1559–1567, 2018. 1
- [10] Qian Da, Xiaodi Huang, Zhongyu Li, Yanfei Zuo, Chenbin Zhang, Jingxin Liu, Wen Chen, Jiahui Li, Dou Xu, Zhiqiang Hu, et al. Digestpath: A benchmark dataset with challenge review for the pathological detection and segmentation of digestive-system. *Medical Image Analysis*, 80:102485, 2022. 3, 4
- [11] Tim Dettmers, Artidoro Pagnoni, Ari Holtzman, and Luke Zettlemoyer. Qlora: Efficient finetuning of quantized llms. *Advances in Neural Information Processing Systems*, 36, 2024. 5
- [12] Lori A Erickson, Ozgur Mete, C Christofer Juhlin, Aurel Perren, and Anthony J Gill. Overview of the 2022 who classification of parathyroid tumors. *Endocrine Pathology*, 33(1):64–89, 2022. 1
- [13] Jevgenij Gamper and Nasir Rajpoot. Multiple instance captioning: Learning representations from histopathology textbooks and articles. In *Proceedings of the IEEE/CVF conference on computer vision and pattern recognition*, pages 16549–16559, 2021. 4, 6, 7
- [14] Zhengrui Guo, Jiabo Ma, Yingxue Xu, Yihui Wang, Liansheng Wang, and Hao Chen. Histgen: Histopathology report generation via local-global feature encoding and cross-modal context interaction. In *International Conference on Medical Image Computing and Computer-Assisted Intervention*, pages 189–199. Springer, 2024. 1
- [15] Chu Han, Xipeng Pan, Lixu Yan, Huan Lin, Bingbing Li, Su Yao, Shanshan Lv, Zhenwei Shi, Jinhai Mai, Jiatai Lin, et al. Wsss4luad: Grand challenge on weakly-supervised tissue semantic segmentation for lung adenocarcinoma. *arXiv preprint arXiv:2204.06455*, 2022. 4
- [16] Zhi Huang, Federico Bianchi, Mert Yuksekogul, Thomas J Montine, and James Zou. A visual–language foundation model for pathology image analysis using medical twitter. *Nature medicine*, 29(9):2307–2316, 2023. 2, 3, 5, 6, 7, 8
- [17] Wisdom Ikezogwo, Saygin Seyfioglu, Fatemeh Ghezloo, Dylan Geva, Fatwir Sheikh Mohammed, Pavan Kumar Anand, Ranjay Krishna, and Linda Shapiro. Quilt-1m: One million image-text pairs for histopathology. *Advances in neural information processing systems*, 36, 2024. 2, 3, 5, 6, 7, 8
- [18] Sajid Javed, Arif Mahmood, Iyyakutti Iyappan Ganapathi, Fayaz Ali Dharejo, Naoufel Werghi, and Mohammed Benamoun. Cclip: Zero-shot learning for histopathology with comprehensive vision-language alignment. In *Proceedings of the IEEE/CVF Conference on Computer Vision and Pattern Recognition*, pages 11450–11459, 2024. 3
- [19] Ting Jiang, Minghui Song, Zihan Zhang, Haizhen Huang, Weiwei Deng, Feng Sun, Qi Zhang, Deqing Wang, and Fuzhen Zhuang. E5-v: Universal embeddings with multimodal large language models. *arXiv preprint arXiv:2407.12580*, 2024. 2, 4, 5, 6, 7, 8
- [20] Jakob Nikolas Kather, Niels Halama, and Alexander Marx. 100,000 histological images of human colorectal cancer and healthy tissue. *Zenodo*10, 5281(9), 2018. 4
- [21] Jakob Nikolas Kather, Johannes Krisam, Pornpimol Charoentong, Tom Luedde, Esther Herpel, Cleo-Aron Weis, Timo Gaiser, Alexander Marx, Nektarios A Valous, Dyke Ferber, et al. Predicting survival from colorectal cancer histology slides using deep learning: A retrospective multicenter study. *PLoS medicine*, 16(1):e1002730, 2019. 4
- [22] Sepideh Khalilboroujeni, Xiangjian He, Wenjing Jia, and Saeed Amirgholipour. End-to-end metastasis detection of breast cancer from histopathology whole slide images.

- Computerized Medical Imaging and Graphics*, 102:102136, 2022. 1
- [23] Katharina Kriegsmann, Frithjof Lobers, Christiane Zgorzel-ski, Jörg Kriegsmann, Charlotte Janßen, Rolf Rüdinger Meliß, Thomas Muley, Ulrich Sack, Georg Steinbus, and Mark Kriegsmann. Deep learning for the detection of anatomical tissue structures and neoplasms of the skin on scanned histopathological tissue sections. *Frontiers in Oncology*, 12:1022967, 2022. 3, 4
- [24] Ritika Kundra, Hongxin Zhang, Robert Sheridan, Sahusapont Joseph Sirintrapun, Avery Wang, Angelica Ochoa, Manda Wilson, Benjamin Gross, Yichao Sun, Ramyasree Madupuri, et al. Oncotree: a cancer classification system for precision oncology. *JCO clinical cancer informatics*, 5: 221–230, 2021. 1
- [25] Feng Li, Renrui Zhang, Hao Zhang, Yuanhan Zhang, Bo Li, Wei Li, Zejun Ma, and Chunyuan Li. Llava-next-interleave: Tackling multi-image, video, and 3d in large multimodal models. *arXiv preprint arXiv:2407.07895*, 2024. 2, 5
- [26] Junnan Li, Dongxu Li, Caiming Xiong, and Steven Hoi. Blip: Bootstrapping language-image pre-training for unified vision-language understanding and generation. In *International conference on machine learning*, pages 12888–12900. PMLR, 2022. 2
- [27] Haotian Liu, Chunyuan Li, Yuheng Li, and Yong Jae Lee. Improved baselines with visual instruction tuning. In *Proceedings of the IEEE/CVF Conference on Computer Vision and Pattern Recognition*, pages 26296–26306, 2024. 2
- [28] Haotian Liu, Chunyuan Li, Qingyang Wu, and Yong Jae Lee. Visual instruction tuning. *Advances in neural information processing systems*, 36, 2024. 2
- [29] Ming Y Lu, Drew FK Williamson, Tiffany Y Chen, Richard J Chen, Matteo Barbieri, and Faisal Mahmood. Data-efficient and weakly supervised computational pathology on whole-slide images. *Nature biomedical engineering*, 5(6):555–570, 2021. 1
- [30] Ming Y Lu, Bowen Chen, Andrew Zhang, Drew FK Williamson, Richard J Chen, Tong Ding, Long Phi Le, Yung-Sung Chuang, and Faisal Mahmood. Visual language pre-trained multiple instance zero-shot transfer for histopathology images. In *Proceedings of the IEEE/CVF conference on computer vision and pattern recognition*, pages 19764–19775, 2023. 1, 2, 3
- [31] Ming Y Lu, Bowen Chen, Drew FK Williamson, Richard J Chen, Ivy Liang, Tong Ding, Guillaume Jaume, Igor Odintsov, Long Phi Le, Georg Gerber, et al. A visual-language foundation model for computational pathology. *Nature Medicine*, 30(3):863–874, 2024. 1, 2, 3, 4, 5, 7
- [32] Jiabo Ma, Zhengrui Guo, Fengtao Zhou, Yihui Wang, Yingxue Xu, Yu Cai, Zhengjie Zhu, Cheng Jin, Yi Lin Xinrui Jiang, Anjia Han, et al. Towards a generalizable pathology foundation model via unified knowledge distillation. *arXiv preprint arXiv:2407.18449*, 2024. 1
- [33] Hui Qu, Mu Zhou, Zhennan Yan, He Wang, Vinod K Rustgi, Shaoting Zhang, Olivier Gevaert, and Dimitris N Metaxas. Genetic mutation and biological pathway prediction based on whole slide images in breast carcinoma using deep learning. *NPJ precision oncology*, 5(1):87, 2021. 1
- [34] Alec Radford, Jong Wook Kim, Chris Hallacy, Aditya Ramesh, Gabriel Goh, Sandhini Agarwal, Girish Sastry, Amanda Askell, Pamela Mishkin, Jack Clark, et al. Learning transferable visual models from natural language supervision. In *International conference on machine learning*, pages 8748–8763. PMLR, 2021. 2, 3, 5
- [35] Mehmet Saygin Seyfioglu, Wisdom O Ikezogwo, Fatemeh Ghezloo, Ranjay Krishna, and Linda Shapiro. Quilt-llava: Visual instruction tuning by extracting localized narratives from open-source histopathology videos. In *Proceedings of the IEEE/CVF Conference on Computer Vision and Pattern Recognition*, pages 13183–13192, 2024. 4, 7, 8
- [36] Julio Silva-Rodríguez, Adrián Colomer, María A Sales, Rafael Molina, and Valery Naranjo. Going deeper through the gleason scoring scale: An automatic end-to-end system for histology prostate grading and cribriform pattern detection. *Computer methods and programs in biomedicine*, 195: 105637, 2020. 3, 4
- [37] Andrew H Song, Drew FK Williamson, and Faisal Mahmood. Investigating morphologic correlates of driver gene mutation heterogeneity via deep learning. *Cancer Research*, 82(15):2672–2673, 2022. 1
- [38] Yuxuan Sun, Chenglu Zhu, Sunyi Zheng, Kai Zhang, Lin Sun, Zhongyi Shui, Yunlong Zhang, Honglin Li, and Lin Yang. Pathasst: A generative foundation ai assistant towards artificial general intelligence of pathology. In *Proceedings of the AAAI Conference on Artificial Intelligence*, pages 5034–5042, 2024. 2, 3, 5, 6, 7, 8
- [39] Yuxuan Sun, Chenglu Zhu, Sunyi Zheng, Yunlong Zhang, Honglin Li, and Lin Yang. Context-aware text-assisted multimodal framework for cervical cytology cell diagnosis and chatting. In *2024 IEEE International Conference on Multi-media and Expo (ICME)*, pages 1–6. IEEE, 2024. 1
- [40] Zhikang Wang, Jiani Ma, Qian Gao, Chris Bain, Seiya Imoto, Pietro Liò, Hongmin Cai, Hao Chen, and Jiangning Song. Dual-stream multi-dependency graph neural network enables precise cancer survival analysis. *Medical Image Analysis*, 97:103252, 2024. 1
- [41] Conghao Xiong, Hao Chen, Hao Zheng, Dong Wei, Yefeng Zheng, Joseph JY Sung, and Irwin King. Mome: Mixture of multimodal experts for cancer survival prediction. In *International Conference on Medical Image Computing and Computer-Assisted Intervention*, pages 318–328. Springer, 2024. 1
- [42] Yingxue Xu, Yihui Wang, Fengtao Zhou, Jiabo Ma, Shu Yang, Huangjing Lin, Xin Wang, Jiguang Wang, Li Liang, Anjia Han, et al. A multimodal knowledge-enhanced whole-slide pathology foundation model. *arXiv preprint arXiv:2407.15362*, 2024. 1
- [43] Jiahui Yu, Zirui Wang, Vijay Vasudevan, Legg Yeung, Mojtaba Seyedhosseini, and Yonghui Wu. Coca: Contrastive captioners are image-text foundation models. *arXiv preprint arXiv:2205.01917*, 2022. 2, 3
- [44] Shichuan Zhang, Sunyi Zheng, Zhongyi Shui, Honglin Li, and Lin Yang. Multi-modal learning with missing modality in predicting axillary lymph node metastasis. In *2023 IEEE International Conference on Bioinformatics and Biomedicine (BIBM)*, pages 2395–2400. IEEE, 2023. 1

- [45] Huajun Zhou, Fengtao Zhou, and Hao Chen. Cohort-individual cooperative learning for multimodal cancer survival analysis. *arXiv preprint arXiv:2404.02394*, 2024. 1